THE JOURNAL OF PHYSICAL CHEMISTRY C

Article

pubs.acs.org/JPCC

Spectroscopic Identification of Hydrogen Spillover Species in Ruthenium-Modified High Surface Area Carbons by Diffuse Reflectance Infrared Fourier Transform Spectroscopy

Jeffrey L. Blackburn,*[,†] Chaiwat Engtrakul,[†] Justin B. Bult,[†] Katherine Hurst,[†] Yufeng Zhao,[†] Qiang Xu,[†] Philip A. Parilla,[†] Lin J. Simpson,[†] John-David R. Rocha,[§] Matthew R. Hudson,[‡,∥] Craig M. Brown,[‡,⊥] and Thomas Gennett[†]

[†]National Renewable Energy Laboratory, Golden, Colorado 80401, United States

[‡]Center for Neutron Research, National Institute of Standards and Technology, Gaithersburg, Maryland 20899-6102, United States

[§]School of Chemistry and Materials Science, College of Science, Rochester Institute of Technology, Rochester, New York 14623, United States

[∥]Department of Materials Science and Engineering, University of Maryland, College Park, Maryland 20742-2115, United States

[⊥]Australian Nuclear Science and Technology Organisation, The Bragg Institute, PMB1 Menai, NSW, Australia

Supporting Information

ABSTRACT: In recent years, carbon-based sorbents have been recognized for their potential application within vehicular hydrogen storage applications. One method by which sorbents have been reported to store appreciable hydrogen at room temperature is via a spillover process: where molecular hydrogen is first dissociated by metal nanoparticle catalysts and atomic hydrogen subsequently migrates onto the carbon substrate. Many reports have invoked the spillover mechanism to explain enhancements in reversible room temperature hydrogen uptake for metal-decorated sorbents. However, there is a lack of experimental evidence for the proposed chemical species formed as well as several differing theoretical explanations describing the process. In this report, we utilize diffuse reflectance infrared Fourier transform spectroscopy (DRIFTS) to identify the various chemical species formed upon room temperature H_2 charging of ruthenium-decorated high surface area carbons. Room temperature H_2 loading of a control sample with no ruthenium nanoparticles (Ru NPs) leads to broad reversible peaks in the DRIFTS spectrum that correspond to the vibration−rotation transitions of weakly bound physisorbed hydrogen molecules. In contrast, the sample modified with Ru NPs shows a variety of reversible and irreversible peaks in addition to the physisorbed H_2 peaks. Rigorous experimental and theoretical analysis enables the assignment of the peaks to ruthenium-mediated formation of water, surface hydroxyl groups (R−OH, where R = carbon or ruthenium), and C−H bonds. The low-energy DRIFTS peaks assigned to spillover C−H bonds were additionally confirmed using inelastic neutron spectroscopy. Reversible vibrational peaks consistent with ruthenium-mediated formation of C−H bonds provide much-needed spectroscopic evidence for the spillover process. The results demonstrated here should facilitate future mechanistic investigations of hydrogen sorption on transition metal nanoparticles and high surface area activated carbons.

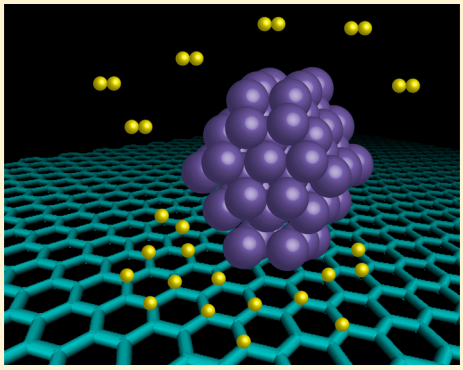

INTRODUCTION

The storage of hydrogen fuel in lightweight low-volume tanks is a necessary, but difficult, prerequisite for the proliferation of hydrogen fuel cell vehicles. Hydrogen storage and release at or near room temperature is ultimately desirable to minimize energetic losses associated with either system cooling (e.g., H_2 storage on weak adsorption materials) or heating (e.g., H_2 desorption from strong adsorption materials). Three primary material sets have been explored over the past decade for vehicular hydrogen storage: metal hydrides, chemical hydrides, and high surface area sorbents.[1,2] While particular examples from each material set are moving closer to achieving DOE targets for volumetric and gravimetric storage capacities, all materials still have drawbacks related to either (or both) the thermodynamics and kinetics of hydrogen sorption and desorption. For example, metal and chemical hydrides employ strong covalent bonds that typically require large energy inputs for desorption,[3,4] while high surface area sorbents rely upon weak physical adsorption (physisorption) of hydrogen molecules and must be cooled to cryogenic temperatures for appreciable adsorption.[5] Activated carbons are an appealing and well-studied material class within hydrogen sorbents, and it has

Received: May 30, 2012
Revised: November 5, 2012
Published: December 17, 2012

been demonstrated that both high surface area and an appropriate pore size distribution are necessary for their high sorption capacities.[6] Ultimately, the sorption capacity of activated carbons is limited to ~6.6 wt % at 77 K, necessitating new approaches to optimize sorption capacities and heats of adsorption for this important class of materials.[7] A hybrid approach, termed hydrogen spillover, has emerged in recent years and combines aspects of metal hydrides and high surface area sorbents.[8−11] The spillover process has been utilized for decades in the catalysis fields[12] and has recently emerged as a potential mechanism for room temperature vehicular hydrogen storage.

The generalized spillover process involves dissociation of molecular hydrogen on a transition metal surface, followed by migration and diffusion of the atomic hydrogen onto a receptor surface.[13] Despite the recent surge in research on spillover for hydrogen storage,[14] there are still large gaps in understanding the fundamental mechanisms at play in the spillover process, especially onto carbon substrates—e.g., the role of surface oxygen groups,[15] thermodynamics associated with the migration and diffusion processes of atomic hydrogen,[16] and ultimate sorbent capacity enhancements achievable through the spillover process.[17] Research on hydrogen spillover onto carbon-based sorbents has primarily taken a phenomenological approach. The prevailing methodology has been to modify high surface area carbons with well-dispersed nanoscale transition metal catalysts and carbonaceous bridging materials such as pyrolyzed sucrose.[11] The carbon sorbents produced in this manner have been reported to adsorb more hydrogen than that expected for a combination of physical adsorption on the carbon surface and surface hydride formation on the metal catalysts. This phenomenological approach relies on the inference that the excess hydrogen can be accounted for by spillover and has been used to suggest that large quantities of dissociated hydrogen may diffuse at ambient temperature on nonmetal supports. However, there is a lack of experimental spectroscopic evidence specifically determining the chemical species formed at the atomic level. Furthermore, there are several different theories as to how H atoms migrate to, diffuse across, and recombine from the carbon support following dissociation on metal NPs.[14,18,19] Spectroscopic identification of unique metal−hydrogen and carbon−hydrogen bonds formed under various sorption/desorption conditions is critical for understanding the fundamental mechanisms involved in the sorbent spillover process. Only once identified can one optimize materials to realize the full potential of the spillover process.

In this report, we utilize diffuse reflectance infrared Fourier transform spectroscopy (DRIFTS) to track surface-adsorbed species following high-pressure (5−100 bar) hydrogen loading of a ruthenium-modified high surface area activated carbon. DRIFTS enables the detection of both physisorbed and chemisorbed hydrogen on a wide variety of materials as a function of pressure and temperature[20−22] and is an ideal tool to explore the mechanistic underpinnings of the spillover process. Infrared absorptive transitions between vibrational levels require a net change in dipole due to the particular vibrational mode in question. This enables one to utilize a broad hydrogen overpressure range since the hydrogen molecule is a linear diatomic molecule for which normal vibrational modes produce no change in dipole; i.e., it will be IR-inactive in its gas phase. However, physisorption of the H_2 molecule to a surface induces asymmetry in the electron cloud, imparting oscillator strength to IR-induced vibrational transitions, allowing physisorption to be tracked by DRIFTS.[20−22] Additionally, and most importantly, metal−hydrogen (M−H) and carbon−hydrogen (C−H) bonds have appreciable IR oscillator strength and can be tracked by DRIFTS.

First, we produce a high surface area boron-doped carbon matrix, which is subsequently decorated with ~1.5 nm ruthenium nanoparticles (Ru NPs) to serve as spillover catalysts. We then utilize DRIFTS to monitor the various surface-adsorbed species resulting from room temperature and elevated temperature hydrogen loading at various pressures in an attempt to discern species that may be formed via spillover. Room temperature H_2 loading of the boron-doped carbon leads to broad peaks that can be assigned to physisorbed molecular hydrogen at >3500 cm^{-1}. In contrast, the Ru NP-modified sample displays a variety of reversible and irreversible peaks (1000−3300 cm^{-1}) *in addition to* the molecular hydrogen physisorption peaks, under the same H_2 loading conditions. A rigorous experimental and theoretical analysis allows us to assign these peaks to the partially reversible formation of water/surface hydroxyls and the reversible formation of "weakened" C−H bonds that are also identified through the application of inelastic neutron scattering. The formation of both water/hydroxyl and C−H bonds is clearly mediated through the ruthenium nanoparticles and can be eliminated by passivation via the generation of covalent Ru−H and C−H bonds. A qualitative analysis of the strength of the "weakened" C−H bonds, along with a relatively small enhancement of adsorption following Ru NP deposition, suggests that the C−H bonds are not likely to be mobile on the carbon surface but instead likely reside adjacent to the Ru NPs.

EXPERIMENTAL/THEORETICAL PROCEDURES

Experimental Procedures. *Sample Identification.* The two samples discussed in detail in this report are the boron-doped carbon and the ruthenium nanoparticle modified boron-doped carbon described in detail below. These samples will be named "BC_X" and "Ru-BC_X", respectively, for the duration of the report.

Synthesis. Synthesis of the boron-doped carbon matrix involved the thermal decomposition of triethylborane ($C_6H_{15}B$) (TEB) onto MSC-30 activated carbon. Spcifically, 500 mg of MSC-30 (BET specific surface area, SSA, ≈3400 m^2/g) is placed into a horizontal tumbler. The tumbler is housed within a 2 in. diameter quartz tube that is surrounded by a horizontal tube furnace. The reaction chamber is evacuated to below 0.13 mbar and purged with argon to 0.66 bar. The evacuation and purge cycle is repeated three times to ensure proper environment for deposition. The chamber pressure is then maintained at 0.66 bar under flowing argon at 200 standard cubic centimeters per minute (sccm). With the tumbler/MSC-30 placed at the center of the furnace, the temperature is raised to 800 °C at 25 °C/min ramp rate. At 800 °C the gas flow is switched to flow through a sealed bubbler containing TEB. The tumbler and sample are then moved forward from the furnace center to the furnace entrance and agitated (rotated ±90°) to receive uniform TEB deposition onto the MSC-30 substrate. After 1 min of deposition, the tumbler is drawn back into the furnace center position to decompose the TEB onto the MSC-30 template. This 1 min deposition/thermal decomposition cycle is repeated every 10 min (1 min deposition for every 9 min of thermal decomposition) for 90 min. After 90 min the flow is returned to pure argon and the furnace is turned off, allowing the

dx.doi.org/10.1021/jp305235p | J. Phys. Chem. C 2012, 116, 26744−26755

temperature to naturally cool to 25 °C. The material is removed from the furnace for characterization and for deposition of Ru NPs.

Ru nanoparticles were deposited onto the BC_X material by microwave deposition. Prior to Ru NP deposition, the base BC_X material was degassed under high vacuum to 275 °C for 4 h with a temperature ramp of 2 °C/min, to eliminate surface oxides species. In order to make 2 g of Ru-BC_X material, 10 separate batches were performed. The NP deposition process for one batch begins with sonication of 200 mg of BC_X material in 10 mL of acetone for 20 min. In a separate vessel, 40 mg of $RuCl_3$ was dissolved and sonicated in 20 mL of acetone for 20 min. The two solutions were then combined and sonicated for an additional hour to ensure the Ru precursor was uniformly dispersed. All sonication was performed in a chilled water bath.

The solution was then heated in a CEM Discover microwave, at fixed power at 250 W under constant stirring. The reaction was stopped after ∼2 min when the pressure of the solution reached 17.2 bar. The solution was then cooled and vented. The resulting solution was then centrifuged and washed with acetone three times, and the remaining powder was dried overnight in a tube furnace at 120 °C under flowing N_2 at 0.66 bar. This was directly followed by a reduction step, by switching the gas to 50 sccm of H_2 at 0.66 bar and ramping the temperature 2 °C/min to 240 °C and held there for 2 h. The deposition resulted in material with uniformly dispersed Ru particles sized between 1 and 3 nm, and the final metal content was 6 wt %.

Sample Characterization. X-ray photoelectron spectroscopy (XPS) was performed on the boron-doped activated carbon, as well as a sample prepared by pyrolysis of only TEB, to determine boron content. XPS spectra were acquired using a Kratos Axis Nova XPS instrument. Although the pure TEB source contains 14% boron (relative to carbon), pyrolysis of TEB was found to produce a boron-doped carbon with 8% boron. The boron-doped carbon utilized for the studies discussed in this report (BC_X sample) was found to contain 4% boron. However, it is likely that the majority of boron is found at or near the surface, since XPS analysis demonstrated that pure TEB pyrolysis produced a carbon with 8% boron.

Nitrogen physisorption was performed to determine the specific surface area of the samples. Nitrogen physisorption was performed on a Micromeritics ASAP 2020 BET instrument. The samples were first degassed to 150 °C over 3 h at a base pressure of 1.33×10^{-11} bar and were then transferred to the BET instrument for standard physisorption analysis. Sample masses were in the 15−20 mg range. A Mettler-Toledo UMT2 microbalance with a readability of 0.1 μg and a repeatability of 0.25 μg was used to determine the mass of each sample used for BET and adsorption isotherms. Consequently, the error introduced into the calculation of BET surface area from weighing small sample masses is only ∼1%. The surface area of the initial BC_X sample was 1800 m^2/g and decreased to ∼1600 m^2/g following the Ru NP deposition procedure.

High-resolution transmission electron microscopy (HRTEM) was acquired on a Phillips CM200 FEG with a 200 keV beam. Energy dispersive X-ray analysis (EDX) was performed in the same instrument, with a Princeton Gamma-Tech Prism EDX spectrometer. The TEM grids were prepared by first sonicating the powders in acetone in a bath sonicator and then dropping the solution onto a lacey carbon TEM grid.

High-Pressure Adsorption Measurement. High-pressure hydrogen capacity measurements were performed on a modified commercial Sieverts system (PCTPro 2000), as described previously.[23] We have modified the commercial system by adding a manifold to the high-pressure gas inlet that allows either hydrogen or helium to be introduced. In this way, exactly the same protocol is used for the hydrogen measurements and for the helium calibration procedure (vide infra). We have also expanded the temperature-controlled region to include the sample support arm and the sample chamber assembly (sample chamber, manual isolation valve, and 0.125 in. OD connection tubing) using temperature-controlled water circulating through copper components physically connected to the sample chamber assembly. This modification greatly improves the overall temperature stability of the apparatus, by ensuring that the temperatures of the internal cabinet and the external circulator are equal. For ambient temperature measurements (303 K), the sample chamber was immersed in stirred water in a double-jacketed dewar (DJD) where the circulator water flowed through the jacket. An OFHC split copper cylinder was clamped to the 0.125 in. tubing so that the copper extended up to the other copper components with active 303 K circulation and was always partially submerged in the stirred water of the DJD. This copper piece helps to extend the 303 K temperature control up from the DJD. Another split copper cylinder was clamped to the 0.125 in. tubing just above lower copper cylinder, and the 303 K circulator water passed through this upper copper cylinder. In this way, the entire sample chamber assembly was actively maintained at 303 K. All these measures ensured that the entire apparatus (including the sample) was isothermal at 303 K and that this was stable and reproducible for the various measurements and helium calibrations.

Samples were first "activated" to reduce oxygen-containing functionalities. For the activation procedure, the powder was placed in a quartz boat inside a quartz tube within a tube furnace. The sample quartz tube was initially evacuated for 10 min at 30 °C to a pressure of 8×10^{-5} bar. Then a continuous flow (0.3 L min^{-1}) of He is allowed into the system at a constant pressure of 7×10^{-4} bar, and the temperature is increased to 150 °C at 2 °C/min. At 150 °C, the gas is changed from He to pure hydrogen at (0.1 L min^{-1}) and controlled at 7×10^{-4} bar. The temperature is then increased to 250 °C at 5 °C/min and held at 250 °C for 3 h under a continuous flow of H_2. After 3 h at a constant temperature 250 °C, the sample was cooled under H_2 gas flow to 30 °C (1 h). The gas flow was stopped, and the chamber was thrice filled/evacuated with helium. At this stage, the sample can be manipulated under air.

The samples were then loaded into tubes designed for the PCT apparatus and were transferred to a custom temperature-programmed desorption (TPD) apparatus for degassing. Samples were degassed by ramping the temperature to 275 °C under dynamic vacuum (1×10^{-11} bar) for 1 h, holding the temperature at 275 °C for 8 h, and then returning the sample to room temperature. Since the sample chamber assembly has a manual isolation valve, the sample chamber can be transferred between the degassing station and the Sieverts apparatus without exposure to air. Adsorption experiments were performed on samples without air exposure and with air exposure to probe the effect of air exposure on adsorption/desorption. The Sieverts protocol consisted of the following sequence after the degassing was accomplished: (1) Measure hydrogen capacity of sample at 303 K. (2) Perform helium calibration at 303 K with sample present to determine the free space calibration. For each measurement step, the pressure was

held for 2 h to allow the sample to come to equilibrium. For adsorption, the first hydrogen overpressure is at ∼20 bar, and the pressure is typically increased in ∼20 bar increments. For desorption, the overpressure is reduced in ∼20 bar increments. The helium adsorption that occurs at 303 K is assumed to be negligible from necessity as it is very difficult to accurately determine this adsorption and compensate for its effects on the hydrogen adsorption determination. Not compensating for helium adsorption effects will yield capacity measurements that *underestimate the hydrogen adsorption*. As mentioned above, because of the modification that allows helium to be introduced into the high-pressure port of the instrument, the same measurement protocol used for hydrogen can also be done with helium albeit with shorter equilibrium times. This provides a higher degree of confidence for the helium calibration and can also investigate any calibration effects dependent on pressure.

Data analysis to determine hydrogen capacities was performed using custom analysis procedures to ensure the highest accuracy. The analysis is based on a mass-balance model of the gas phase where missing gas is assumed to be adsorbed onto the sample and surplus gas is assumed to have desorbed from the sample. A real equation of state was used for the gases and the compressibility factor was based on calculations using GASPAK for helium and hydrogen.

Diffuse Reflectance Infrared Transmittance Spectroscopy (DRIFTS). DRIFTS measurements were performed on a Thermo-Nicolet 6700 FTIR spectrometer fit with high pressure/high temperature DRIFTS cell. A Thermo Spectra Tech Collector II (P/N 700-0042) adapter was used to modify the spectrometer for reflection measurements, and the DRIFTS sample holder was a Thermo Spectra Tech High Temperature/Vacuum Chamber (P/N 0030-103) with ZnSe windows. The DRIFTS spectra displayed in this article were acquired using 1024 scans for both the background and the sample scan. For a given series of spectra, the background scan was performed at ∼5 psi H_2 loading (0.3 bar). All spectra shown (except for Figure 7a) were baseline-corrected to remove any gradual sloping changes in the spectral baseline.

Samples were transferred to the DRIFTS measurement following high-pressure adsorption measurements on the PCT Pro. Samples were briefly exposed to air before DRIFTS measurement so that the DRIFTS measurement could identify any species formed as a result of this air exposure, in addition to any species formed by hydrogen spillover. Before DRIFTS measurements, the sample was degassed externally on the TPD apparatus. This degas step consisted of a 2 h ramp to 200 °C under dynamic vacuum following evacuation to a base pressure of $\sim 2.6 \times 10^{-11}$ bar. Following the degas step, the sample holder was anaerobically transferred into an inert glovebox (He atmosphere, <0.1 ppm O_2 and H_2O). The sample was loaded into the DRIFTS sample cup inside the glovebox, after which the DRIFTS cell was completely sealed, removed from the glovebox, and then attached to the DRIFTS spectrometer. Note: in the DRIFTS a doublet at 2280 cm^{-1} is seen in many spectra and is due to incomplete subtraction of CO_2. Because of slight deviations in backgrounds, these peaks may appear as an upward or downward pointing doublet and in some cases may not appear above the noise.

Inelastic Neutron Scattering. A 316-stainless steel (SS) cylindrical cell was specially designed for use in a closed-cycle refrigerator (CCR) for neutron scattering measurements and under operating pressures of 100 bar. The SS cell had a 1/8 in. SS capillary line welded for the addition of hydrogen gas to the sample and monitoring the pressure. The assembly was vacuum-tested to a vacuum tolerance of 10^{-9} mbar and pressure tested to 90 bar. 1.85 g of Ru-BC_X was loaded into the cell for measurement. The sample was activated *in situ* in the SS cell. The cell temperature was raised to 275 °C ramping at 1 °C/3 min (12 h total) and then cooled to room temperature (RT) all the while under dynamic vacuum. At room temperature, 1 bar of hydrogen was added, and the heating cycle was repeated under dynamic vacuum.

Inelastic neutron scattering (INS) spectra were collected on the BT-4 Filter-Analyzer Neutron Spectrometer (FANS) at the NIST Center for Neutron Research (NCNR).[24] A copper (220) monochromator allows energy transfers between 35 and 175 meV (280−1400 cm^{-1}) to be easily achieved. A background measurement of the bare Ru-BC_X sample in the SS cell was made over 2 days at RT. Hydrogen gas was allowed to saturate the sample volume at a regulated pressure of ≈22 bar (319 psi) for another 10 days. An INS spectrum of the H_2 loaded Ru-BC_X (+ SS cell) was collected from 35 to 175 meV over a further 2 days. The sample was removed from the SS cell, and the INS spectra of the empty SS cell and the SS cell dosed with ≈22 bar (319 psi) of H_2 at RT were each measured for a day. Data were reduced using the DAVE[25] suite of programs. The excess hydrogen scattering due to hydrogen exposure (spillover) was calculated by subtracting the (activated Ru-BC_X + cell) measurement and the (H_2 + cell) − (cell only) spectra from the SS cell with the hydrogen loaded Ru-BC_X spectrum.

Theoretical Methods. We performed first-principles calculations to help identify the peaks observed in DRIFTS and neutron scattering experiments. To mimic the experimentally synthesized materials, we considered the model system of a graphene fragment with 28 carbon atoms with each of the 14 edge C atoms terminated by an H atom, i.e., $C_{28}H_{14}$. Boron doping was studied by replacing a C atom in the middle of the fragment with a boron atom, i.e., $C_{27}BH_{14}$. One weakly chemisorbed H atom was added to a C atom in the middle of the sheet fragments. Employing the DFT method with B3LYP[26] exchange-correlation potential and the 3-21G basis set[27] as implemented in Gaussian 09 package,[28] we optimize the atomic structures of the undoped and boron-doped graphene fragments. Vibration frequencies were calculated with the Hessian matrix method. The neutron scattering spectra are generated within the DAVE suit of programs[25] with the components of vibrational motion identified from the eigenvectors.

RESULTS AND DISCUSSION

Figure 1A shows a high-resolution TEM image of the Ru-BC_X sample used in this study. Well-dispersed ruthenium nanoparticles (Ru NPs) with diameters between approximately 1 and 3 nm are visible as dark spots adhering to the BC_X-carbon substrate. Several recent studies have demonstrated that the diameter and dispersion of the metal nanoparticles on the carbon substrate are critical parameters for the realization of spillover, and small diameters (<4 nm) with good dispersion are essential.[29,30] Thus, the well-dispersed, very small Ru NPs observed in Figure 1A for Ru-BC_X sample should be suitable for spillover. It is important to briefly discuss our choice of a boron-doped activated carbon substrate over an undoped activated carbon. Many recent studies, by our group and others, have shown that substitutional dopants (both nitrogen and boron) aid in both the uniformity of nanoparticle dispersion on

dx.doi.org/10.1021/jp305235p | J. Phys. Chem. C 2012, 116, 26744−26755

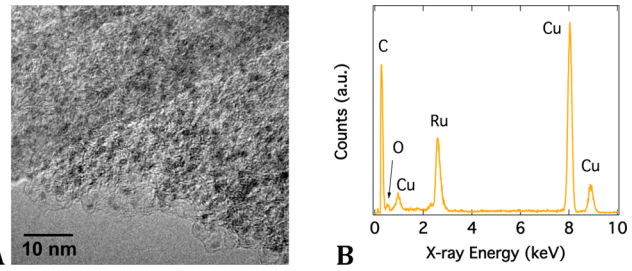

Figure 1. (A) High-resolution TEM image of a Ru-BC_X sample, showing well-dispersed Ru nanoparticles with average size of ~1.5 nm. (B) EDX of the same area showing that the sample consists of carbon, ruthenium, and some oxygen due to surface functional groups.

carbon substrates *and* the stability of the nanoparticles under adverse operating conditions (e.g., elevated temperatures or under potential cycling).[31−33] Theoretical treatments demonstrate that the empty p orbitals of boron atoms aid in the coordination of transition metal atoms (with d orbital electrons to donate) to the carbon substrate, and the bound metal particles are found to be more stable on boron sites.[34,35] These theoretical treatments have been validated by a number of experiments that use TEM and SEM to quantify the dispersion (particle size and number density) and stability of Pt, Ru, and alloy nanoparticles on HOPG substrates and activated carbons that are doped with either B or N.[31−33] Additionally, from our experience with the MSC-30 activated carbon used here, we routinely achieve better dispersion of smaller Ru nanoparticles on the boron-doped MSC-30 relative to the undoped MSC-30 substrate. We have also found significantly lower levels of spillover-related enhancements on undoped MSC-30 substrates, with less reproducible results.

Figure 1B shows the energy dispersive X-ray (EDX) spectrum obtained from the area shown in Figure 1A. Several copper peaks are present from the copper TEM grids at 0.95, 8.0, and 8.9 keV. Strong ruthenium peaks are present at 2.57 and 19.3 keV (not shown), and a strong carbon peak is present at 0.28 keV. Additionally, a small oxygen peak can be observed at 0.31 keV. This peak varies in intensity for various spots on the sample and indicates a variable amount of oxygen-containing surface functional groups on the sample.

Figure 2A compares the high-pressure adsorption isotherms of the BC_X (red circles) and Ru-BC_X materials. Two isotherms are displayed for the Ru-BC_X material. For each Ru-BC_X isotherm, the sample was first "activated" by heating to 200 °C in a 14 bar H_2 overpressure in an attempt to reduce any oxidized Ru metal surfaces as well as oxygen-containing functional groups on the carbon substrate. Following this activation, the sample were then heated to 250 °C in vacuum to desorb any species formed in the activation process. The blue diamonds display the isotherm of this "activated" Ru-BC_X sample. A clear enhancement of H_2 uptake is seen for this Ru-BC_X sample relative to the BC_X sample. At a pressure of ~50 bar, this enhancement is 18 ± 2%. The sample was then exposed to lab air before the H_2 adsorption measurement, producing the isotherm that is shown as the green squares. For the sample that was exposed to air prior to H_2 adsorption, there is a significant increase in the measured H_2 uptake of ~40% relative to the BC_X control sample (at 50 bar), a significantly larger enhancement relative to the sample that was not air-exposed. Following this measurement, the sample was degassed under vacuum while monitoring gas evolution (Figure 2B). Evolution of H_2O was clearly observed by the large signal at 18 amu, explaining the additional H_2 capacity following air exposure. Importantly, these data demonstrate that erroneous adsorption enhancements related to the formation of water and surface hydroxyls could be mistakenly attributed to a spillover phenomenon. This concept is revisited below regarding the discussion of DRIFTS data.

Figure 3 displays DRIFTS spectra of BC_X and Ru-BC_X at hydrogen overpressures of 14 bar (Figure 3A) and 41 bar (Figure 3B). At 14 bar, the BC_X spectrum contains only a broad peak envelope between ~3500 and 6000 cm^{-1}, in which two broad peaks can faintly be made out. By 41 bar, the BC_X spectrum shows the same broad peak envelope, but a broad triplet is clearly discernible within this peak envelope, with peaks at 4190, 4550, and 4750 cm^{-1}. These peaks arise from vibration−rotation transitions corresponding to the Q_1, $S_1(0)$, and $S_1(1)$ branches for hydrogen molecules that are physisorbed to the BC_X material.[20,36] Since H_2 is a linear diatomic molecule, these transitions are forbidden in the gas phase since there is no change in dipole induced by these molecular vibrations. Physisorption of hydrogen molecules to a surface, however, induces asymmetry to the H−H electron cloud that imparts oscillator strength to these transitions.[20] The area underneath the $Q_1/S_1(0)/S_1(1)$ peak envelope increases with increasing H_2 overpressure, as is consistent for Langmuir-like physisorption of H_2 on an activated carbon.

DRIFTS spectra for Ru-BC_X following 14 and 41 bar H_2 charging are significantly different than the BC_X spectra (Figure

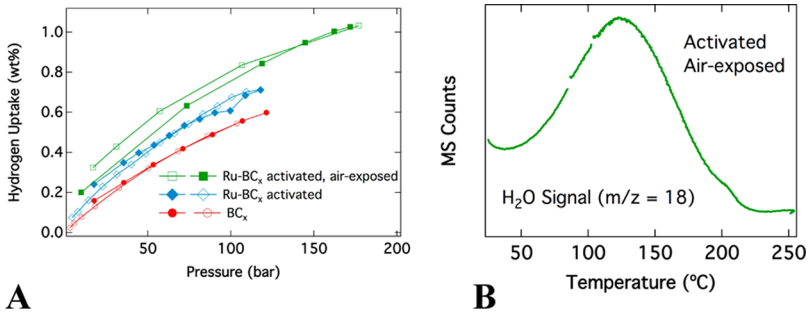

Figure 2. (A) High pressure (T = 303 K) H_2 adsorption isotherms of BC_X control sample (red circles), Ru-BC_X sample that has been exposed to air before the adsorption measurement (green squares), and a Ru-BC_X sample that was first treated with H_2 and then degassed, prior to adsorption measurement (with no air exposure, blue diamonds). Filled points are for adsorption and open points are for desorption (B) Temperature-programmed desorption of the Ru-BC_X sample that was exposed to air before the H_2 adsorption measurement, demonstrating that the high-pressure H_2 dose forms a significant amount of water via reduction of surface oxides.

dx.doi.org/10.1021/jp305235p | J. Phys. Chem. C 2012, 116, 26744−26755

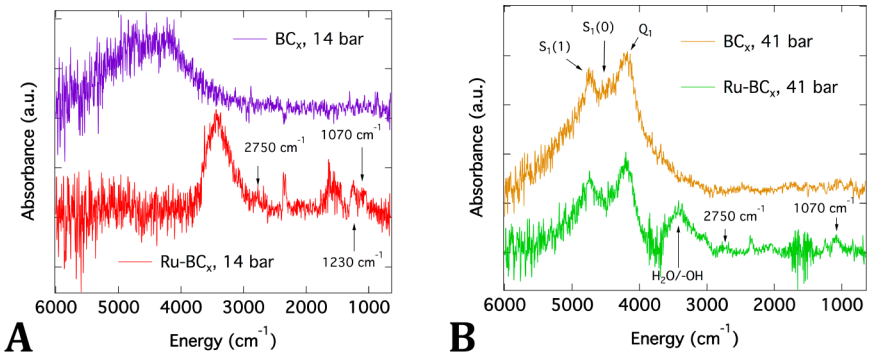

Figure 3. (A) Comparison of BC_X and Ru-BC_X DRIFTS spectra following room temperature H_2 charging at 14 bar. (B) Comparison of BC_X and Ru-BC_X DRIFTS spectra following room temperature H_2 charging at 41 bar. In each spectrum, the unique peaks observed on the Ru-BC_X sample at 2750, 1230, and 1070 cm^{-1} are labeled.

3). We first note that the air-exposed Ru-BC_x sample measured here was degassed in vacuum following air exposure, but did not undergo a subsequent H_2 "activation" step to reduce surface oxides. At 14 bar, the spectrum contains several features above ~1300 cm^{-1} that can be assigned to water formation. The broad peak at 3400 cm^{-1} is similar to the peak seen in liquid water at room temperature, which contains contributions from the symmetric stretching mode (ν_1), antisymmetric stretching mode (ν_3), and an overtone of the bending mode (ν_2) of O−H bonds. Additionally, a peak is observed around 1600 cm^{-1}, indicative of the bending mode (ν_2) of O−H bonds. This peak is surrounded on either side by some noise due to the background suppression feature of the DRIFTS spectrometer, which attempts to remove contributions from ambient water molecules. The formation of these peaks on the Ru-BC_X sample is a clear indication of water or surface hydroxyl (R−OH) formation and further supports the importance of proper oxide reduction before any attempts to assign adsorption enhancements to spillover (Figure 2). The lack of these peaks in the BC_X sample suggests that the formation of these peaks is mediated specifically through the Ru NPs on the Ru-BC_X sample.

Interestingly, the two peaks below 1300 cm^{-1} (1250 and 1070 cm^{-1}), as well as a peak at 2750 cm^{-1}, are not associated with water formation. In order to establish the origin of these peaks, a series of sorption/desorption experiments were performed. First, it was observed that upon raising the H_2 overpressure to 41 bar the intensities of the 1070 cm^{-1}/1230 cm^{-1} peaks increase while the intensity of the water peak (~3400 cm^{-1}) remains constant. This observation is the first piece of evidence that the 1070 cm^{-1}/1230 cm^{-1} peaks are not related to the water formation.

To probe the behavior of the surface-bound hydrogen species formed on the Ru-BC_X sample in more detail, we performed H_2 sorption/desorption cycling studies. Figure 4 shows a cycling experiment for a second Ru-BC_X sample that was distinct from the sample shown in Figure 3. This sample was a different aliquot from the same large 2 g batch. In this experiment, the H_2 overpressure is successively reduced from 45 bar, after which point the sample cell is evacuated to 1.3 × 10^{-8} bar, and then H_2 is reintroduced up to a pressure of 43 bar. We first note that with increases of the hydrogen overpressure up to 45 bar this sample shows the appearance of the same IR peaks as those observed for the first Ru-BC_X sample shown in Figure 3B. This similarity attests to the reproducibility of the synthesis procedure and DRIFTS

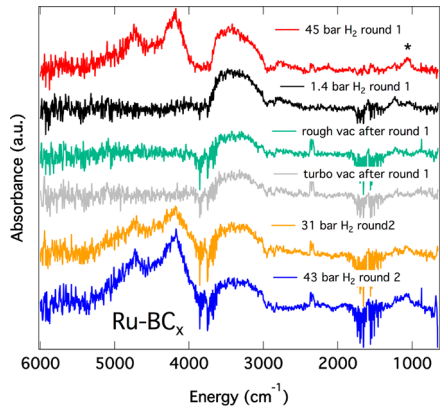

Figure 4. Cycling experiment on Ru-BC_X sample. Sample initially charged with 45 bar H_2 overpressure (red trace), after which the H_2 overpressure reduced to 1.4 bar (black trace). The H_2 was then removed, and the sample chamber was evacuated to a pressure of 10 mTorr with the roughing vacuum (green trace). Next, the pressure was further reduced to ~1.3 × 10^{-8} bar with the turbo pump (gray trace). The sample was recharged with 31 bar of H_2 (orange trace) and then raised up to 43 bar (blue trace). The asterisk marks the position of the 1070 cm^{-1} peak that disappears in the pump-down sequence of round 1 and then reappears with the reintroduction of H_2 in round 2.

measurements and ensures that the peaks are not sample-dependent (within a set of unique Ru-BC_X samples). Upon decreasing the H_2 overpressure from 45 to 1.4 bar, the intensity of the water peak at 3400 cm^{-1} decreases slightly and becomes less sharp. When the sample compartment is evacuated from 1.4 bar to a base pressure of ~1.3 × 10^{-4} bar, the intensity of the water peak is further diminished but does not completely disappear. Even after evacuation with the turbomechanical pump down to a base pressure of ~1.3 × 10^{-8} bar, a small water peak is still present. As the pressure is then raised up to 43 bar, the intensity and shape of this water peak change very little. In contrast, the peaks at 1070 cm^{-1}/1230 cm^{-1} completely disappear upon evacuation and then reappear as H_2 is reintroduced up to 43 bar. The difference in cycling behavior for these peaks and the 3400 cm^{-1} water peak shown in Figure 4 is the second piece of evidence that these peaks arise from different surface species. Finally, as expected for H_2 physisorption, the broad physisorption peak envelope diminishes and disappears as the H_2 pressure is reduced and then reappears with the subsequent H_2 load.

We interpret the DRIFTS spectra for the BC_X and Ru-BC_X materials with the following model. The broad peaks between

dx.doi.org/10.1021/jp305235p | J. Phys. Chem. C 2012, 116, 26744−26755

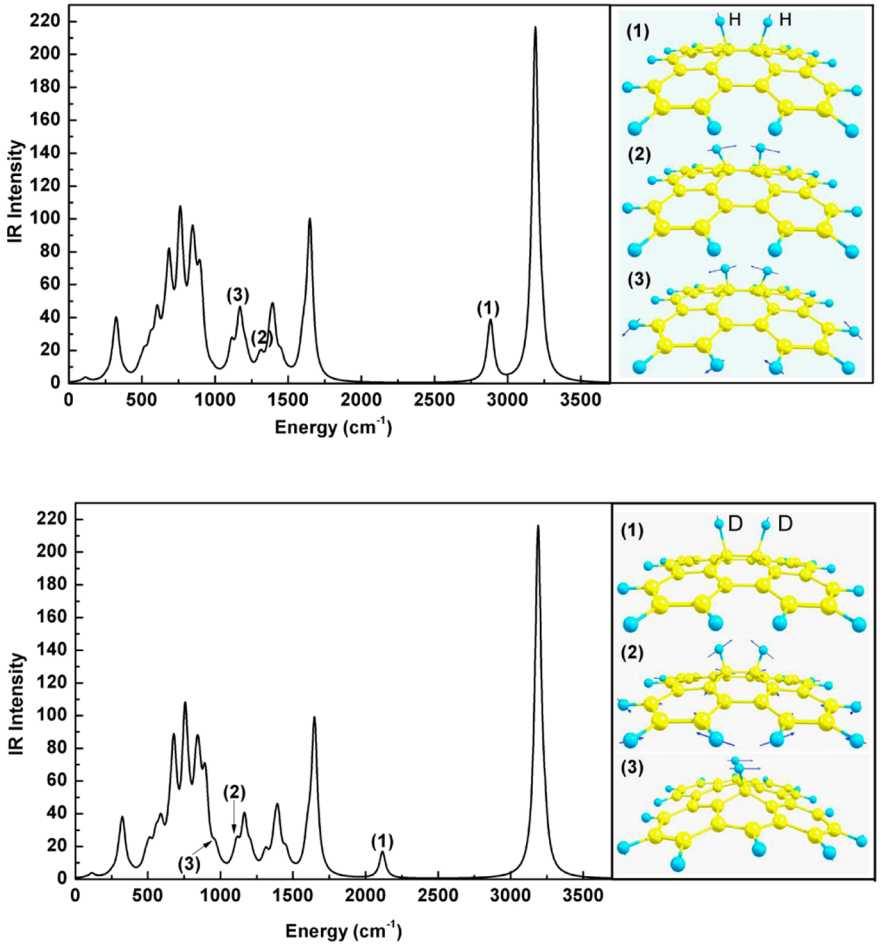

Figure 5. First-principles calculations of vibrational frequencies of H (top) or D (bottom) atoms on graphene (C_{28}) fragments. Left plots show calculated IR spectra of graphene-2H (top) and graphene-2D (bottom). Right plots show three distinct vibrational modes of the H (top) or D (bottom) atoms. The 2881/2114 cm^{-1} peaks (1) correspond to the stretching mode of the C−H/C−D bonds. The 1315/1081 cm^{-1} (2) and 1170/962 cm^{-1} (3) peaks correspond to bending modes of the C−H/C−D bonds.

~3500 and 6000 cm^{-1} clearly correspond to the $Q_1/S_1(0)/S_1(1)$ peaks of H_2 physisorbed within the pore structure of the activated carbons for both samples. The area underneath the physisorption peak envelope is larger for the BC_X material at any given pressure, consistent with the observation that the BET surface area decreases from ~1800 to 1600 m^2/g following Ru deposition. Water formation (~3400 cm^{-1}) is clearly mediated by the ruthenium catalysts on the Ru-BC_X material, as appreciable water is not formed on the metal-free BC_X sample. The cycling behavior of the water peak suggests that two distinct species likely contribute to this broad peak. One species is removed as the H_2 overpressure is reduced and the sample cell is evacuated, while another species remains bound to the surface and is not removed. We conclude that both of these species arise from H_2 reduction of surface oxides. In one case, H_2O is formed that becomes temporarily trapped in the pores of the activated carbon, while some surface oxides are only partially reduced to surface-bound hydroxyls, R−OH. Upon reducing the H_2 overpressure and evacuating the sample cell, physisorbed H_2O is removed from the pore structure, while the surface-bound hydroxyls remain bound to the surface. The remaining surface-bound hydroxyls are responsible for the large fraction of the ~3400 cm^{-1} peak envelope that does not disappear upon removal of the hydrogen overpressure and is not modified by the subsequent hydrogen load in Figure 4. Importantly, this reaction only occurs in the first cycle. Therefore, it follows that H_2 reduction of surface oxides occurs within the first H_2 loading cycle and that these oxides are not active in subsequent cycles. This is entirely consistent with the behavior observed in volumetric H_2 sorption experiments, as shown in Figure 2, and has also recently been observed for other metal−carbon systems such as Pd on activated carbon.[37] In Figure 2, removing the H_2 overpressure is insufficient to return the activated/air-exposed sample to its initial weight (i.e., weight before adsorption), indicating that some hydrogen from the adsorption step cannot be removed. This excess hydrogen can be accounted for by considering the surface-bound hydroxyls demonstrated by DRIFTS to remain on the sample surface upon evacuation (Figure 4). The 1070/1230/2750 cm^{-1} peaks are seen only on the Ru-BC_x sample and display different charging and cycling behavior than observed for the physisorption of H_2 and the formation of water/surface hydroxyls. The species giving rise to these peaks must be mediated by the ruthenium catalyst particles, as these peaks are not observed for the BC_X sample.

In an attempt to identify the species giving rise to the 1070/1230/2750 cm^{-1} peaks, we performed first-principles calculations on model fragments of graphene (C_X) and boron-doped graphene (BC_X). Figure 5 shows graphene patches to which H (top frame) and D (bottom frame) atoms are bound. For H_2−

C_{28}, we observe three important peaks for the normal H−C vibrational modes: the stretching mode with peak frequency at 2881 cm^{-1} (1) and the librational (bending) modes that appear at frequencies of 1315 cm^{-1} (2) and 1170 cm^{-1} (3). These peaks correspond to the normal modes of H atoms bound to the basal plane on the graphene sheet, in a configuration in which the H atoms are on directly adjacent carbons. For D_2−C_{28}, the stretching mode has shifted to 2114 cm^{-1}, while the bending modes have shifted to 1081 and 962 cm^{-1}.

We note that the peak energies predicted for the H_2−C_{28} sample (2881, 1315, and 1170 cm^{-1}) are very close to the peak energies observed experimentally for the Ru-BC_X sample following H_2 loading (2750, 1230, and 1070 cm^{-1}) that were shown to not correspond to water. This similarity suggests that the experimentally observed peaks may correspond to H atoms bound on the "graphene-like" sheets upon exposure of the Ru-BC_X to molecular hydrogen. Since the peaks are only observed for the Ru-BC_X sample, and not for the BC_X sample, the Ru catalysts clearly mediate the formation of these surface-bound hydrogen atoms. This mechanism is consistent with the spillover process, which proposes that hydrogen molecules may be dissociated on small metal nanoparticles, forming hydrogen atoms that subsequently migrate or "spill over" onto the adjacent carbon substrate.

We note that we also ran first-principles calculations on graphene fragments with B atoms substitutionally doped into the graphene lattice, as shown in the Supporting Information. In these calculations, the boron atom is directly adjacent to the carbon atom to which the hydrogen atom adsorbs. For the boron-doped fragments, the energy for the C−H stretch does not change, but the librational modes shift to significantly lower energy (300−700 cm^{-1}). Unfortunately, the transparency of the ZnSe windows used in the DRIFTS experiment drops off dramatically below ∼700 cm^{-1}. Thus, we cannot ascertain any peaks that may arise due to C−H bonds that are locally influenced by the electron-deficient boron dopants. Certainly, there is expected to be significant variation in the local atomic environment within the Ru-BC_X sample, with some regions potentially influenced by the local electronic effects of boron dopants and others in regions dominated solely by the carbon framework. In any case, the correlation that we observe between DRIFTS spectra and DFT calculations on graphene-H fragments (without boron dopants) in which H atoms are bound to the basal plane of graphene leads us to hypothesize that the DRIFTS peaks observed at 2750, 1230, and 1070 cm^{-1} are due to spillover hydrogen atoms.

Each one of the experimentally observed peaks is lower in energy (5%−9%) than the peak energies predicted by first-principle calculations. The vibrational frequency ($\bar{\upsilon}$) of a linear diatomic molecule can be approximated using Hooke's law:

$$\bar{\upsilon} = \frac{1}{2\pi c}\sqrt{\frac{f(m_1 + m_2)}{m_1 m_2}} \quad (1)$$

where c is the speed of light (cm/s), m_1 and m_2 are the atomic masses of each atom in grams, and f is the force constant of the bond (dyn/cm). The force constant is proportional to the strength of the bond between the two atoms, and the vibrational frequency is proportional to the square root of the force constant. Thus, we can approximate the bond energy of the C−H bonds observed experimentally by rearranging eq 1 and comparing to the bond energy predicted by first-principles calculations:

$$\frac{f_1}{f_2} = \left(\frac{\bar{\upsilon}_1}{\bar{\upsilon}_2}\right)^2 \quad (2)$$

In eq 2, f_1 and $\bar{\upsilon}_1$ are the force constant and vibrational frequency for the C−H bonds calculated from first-principles calculations and f_2 and $\bar{\upsilon}_2$ are the force constant and vibrational frequency for the C−H bonds observed experimentally. Using this relationship, we can estimate that the bond energies for the peaks observed experimentally are ∼10−20% lower than the bond energies of the idealized covalent C−H bonds predicted by first-principles calculations. The lower energy of the experimentally observed C−H bonds may arise from structural variations in the Ru-BC_X sample, including varying curvature of the graphitic carbon and the randomness of both graphitic and amorphous regions near the Ru catalyst particles onto which H atoms migrate.[19] These calculations suggest that the bonds formed by the apparent spillover process are weaker than C−H covalent bonds with unstrained sp^3 bonds but still have sufficiently large energies to make subsequent diffusion energetically unfavorable. At this point, we tentatively rationalize the reversibility of these peaks by suggesting that the spillover H atoms form small regions of C−H bonds directly adjacent to the Ru NPs and cannot diffuse large distances over the carbon substrate due to their relatively high binding energies.

Building upon the hypothesis that the DRIFTS measurement resolves infrared absorbance peaks resulting from hydrogen spillover on the Ru-BC_X sample, we designed several experiments to further clarify the origin of these peaks. We first charged the sample with deuterium (D_2), as shown in Figure 6. The spectrum of the D_2-charged sample contains

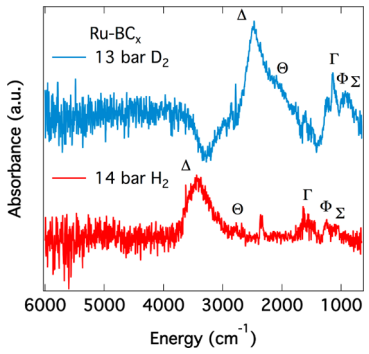

Figure 6. Comparison of D_2 and H_2 charged Ru-BC_X sample. Each sample was charged at room temperature. Roman letters indicate equivalent peaks that shift to lower energy for the D_2-charged sample due to the isotope effect on the vibrational energy.

several interesting features, which we describe in order of descending vibrational frequency. First, a downward pointing broad peak is observed with peak energy at ∼3200 cm^{-1}, suggesting a diminishment of the surface concentration of a particular surface-bound species. Correlation with the H_2-charged sample allows us to assign this peak to surface-bound hydroxyls (R−OH), in which D atoms replace H atoms upon charging with D_2. A large absorbance is observed at 2480 cm^{-1} (labeled Δ), with a broad shoulder in the range of ∼1900−2100 cm^{-1}. The 2480 cm^{-1} peak is consistent with the formation of surface-bound R−OD moieties since an isotope-induced shift of ∼950 cm^{-1} would be expected for hydroxyl species, based on the relative masses of D and H. Furthermore,

dx.doi.org/10.1021/jp305235p | J. Phys. Chem. C 2012, 116, 26744−26755

a sharp peak is observed at 1200 cm^{-1}, corresponding to the bending mode (ν_2) of OD bonds. The corresponding mode for the H_2-charged sample occurs at 1600 cm^{-1}, and is labeled Γ in Figure 6. Returning to the shoulder observed between ∼1900 and 2100 cm^{-1} (Θ), the peak of this shoulder, estimated by deconvolution, is found to be ∼2010 cm^{-1}. This is ∼5% lower than the vibrational frequency predicted for the C−D stretching frequency of the graphene-D model system shown in Figure 5 (2114 cm^{-1}). The lower frequency of the experimentally observed peak relative to that predicted by first principles is entirely consistent with the behavior of the peak observed at 2750 cm^{-1} for the H_2-charged sample and confirms the assignment of the 2750 and 2010 cm^{-1} peaks to C−H and C−D stretching, respectively.

Moving to lower frequency, we observe two peaks for the D_2-charged sample below 1300 cm^{-1} that do not correspond to water/hydroxyl (R−OD) formation. As discussed above, the sharp 1200 cm^{-1} peak is assigned to the ν_2 mode of OD bonds. We also observe a broad peak at ∼920 cm^{-1} for the D_2-charged sample, which is ∼5% lower than the frequency predicted by first-principles calculations for the wagging mode of the C−D bond in the graphene-D model system (962 cm^{-1}). This peak is consistent with the isotope-induced shift of the 1070 cm^{-1} peak observed for the H_2-charged sample (Σ), although it is significantly broader. Thus, we suggest a broad envelope peaking at ∼920 cm^{-1} for the D_2-charged sample resulting from two overlapping peaks, the isotope-induced shifts of both the 1230 cm^{-1} (Φ) and 1070 cm^{-1} (Σ) peaks, which have reduced interpeak spacing in the D_2-charged sample. As such, this broad peak is labeled with both Φ and Σ. A full correlation of the isotope-induced peak shifts with the calculations of Figure 5 allow us to interpret these peaks to the bending modes of C−H/C−D bonds. Thus, the D_2 charging experiment lends supporting evidence to the hypothesis that weakened C−H/C−D bonds are formed on the carbon substrate for the Ru-BC_X sample and that this process is mediated by the Ru catalyst particles.

Next, we performed an "activation" experiment in which we attempted to block access to ruthenium dissociation sites and acceptor sites on the carbon substrate by forming strong covalent bonds. This experiment consists of first charging the sample with H_2 up to a pressure of 14 bar in the DRIFTS cell and then heating the sample to 200 °C. Figure 7A shows DRIFTS spectra as a function of temperature during this activation procedure. At temperatures above ∼130 °C, several intense peaks begin to emerge; however, the absorbance background clearly changes as a function of temperature, giving rise to a large upward-sloping spectrum at lower energies as the temperature increases. To eliminate this artifact, we measured the DRIFTS spectrum of the "activated" Ru-BC_X sample after the sample had been fully heated to 200 °C under the 14 bar H_2 overpressure and then cooled back down to room temperature. This spectrum is plotted in Figure 7B, along with the spectrum of the Ru-BC_X sample charged with 41 bar of H_2 at room temperature. Note that the magnitude of the peaks observed for the activated sample is nearly 40 times that of the peaks observed for the sample charged at room temperature.

Most notably for the "activated" Ru-BC_X sample, we observe a group of three peaks with frequencies of 3142, 3050, and 2820 cm^{-1} and a very sharp, strong peak at 1406 cm^{-1}. This 1406 cm^{-1} peak has a small shoulder at 1446 cm^{-1}, and two additional weak peaks are observed at 1760 and 2008 cm^{-1}. The 1760 cm^{-1} peak matches very closely with the peak

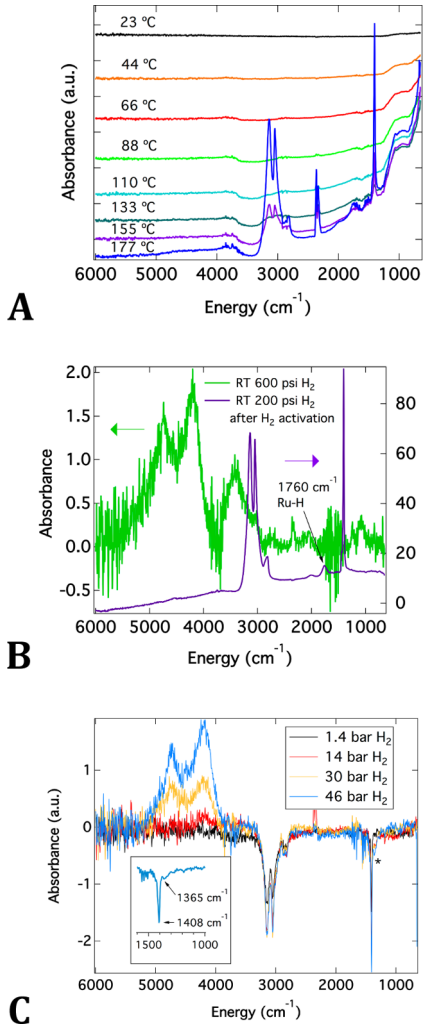

Figure 7. High-temperature H_2 activation experiments on Ru-BC_X sample. (A) Sequential DRIFTS spectra during 120 min ramp to 200 °C under a 14 bar H_2 overpressure. (B) Comparison of activated Ru-BC_X sample after cooling down to room temperature under 14 bar H_2 (purple) to Ru-BC_X sample charged with H_2 at room temperature, 41 bar H_2 (green). (C) Room temperature H_2 charging of activated Ru-BC_X sample following 200 °C, 14 bar H_2 activation. Note that the baseline for the spectra in (C) is the activated sample (purple spectrum in Figure 7(B)). Asterisk marks the position of the small desorption shoulder observed at 1365 cm^{-1}, assigned to bridging Ru−H−Ru species. Inset shows a zoom of this region, highlighting the 1408 and 1365 cm^{-1} desorption peaks. Note that the absorbance values for all *y*-axes of (B) and (C) are multiplied by 1000.

observed by Kubota et al. for hydrogen-charged ruthenium metal particles (1760 cm^{-1} with a shoulder at 1870 cm^{-1}), which was assigned to H atoms adsorbed in an "on-top" position on single ruthenium atoms.[40] The presence of this strong peak at 1760 cm^{-1} indicates that a large number of the surface-exposed ruthenium atoms are bound covalently to hydrogen atoms following the activation procedure. As demonstrated below, this Ru-hydride renders the Ru NPs inactive for potential mediation of any subsequent spillover processes. The other strong peaks observed for the activated sample (2820−3142 cm^{-1} triplet, 1406/1446 cm^{-1} doublet) have not been observed in other reports. However, we note that the peaks in the 2820−3150 cm^{-1} range are in the range expected for covalent C−H bonds or surface-bound hydroxyls

dx.doi.org/10.1021/jp305235p | J. Phys. Chem. C 2012, 116, 26744−26755

(R−OH), while the strong 1406 cm^{-1} peak is in the range expected for either the symmetric C−H deformation or the OH bend of surface hydroxyls. Together, the peaks observed for the activated Ru-BC_X sample indicate that the activation process forms a large quantity of covalent bonds on both the ruthenium nanoparticles and the carbon acceptor substrate that should preclude the subsequent realization of a significant spillover effect (see below).

Following the activation process, a new baseline was taken of the activated sample (purple spectrum, Figure 7(B)), such that subsequent spectral changes could be observed in the absence of the large peaks present for the activated sample. Then, the 14 bar H_2 overpressure was evacuated from the sample cell, and the sample cell was evacuated to 1.3×10^{-8} bar, in preparation for subsequent H_2 loads. We note that only a very small amount (<0.1%) of the covalent bonds formed during the activation process were removed by evacuation to 1.3×10^{-8} bar, as evidenced by a small negative DRIFTS spectrum in the region of ∼3000 cm^{-1} (not shown) after ∼20 min pumping time at 1.3×10^{-8} bar. Following evacuation, the activated sample was charged with molecular hydrogen at room temperature. Figure 7C displays the DRIFTS spectra obtained when the activated Ru-BC_X sample was charged with room temperature molecular hydrogen at pressures of 1.4, 14, 30, and 46 bar. Upon introduction of 1.4 bar of H_2, negative signals are observed in the regions of 2820−3150 and 1400 cm^{-1}, indicating the desorption of a small amount of the covalent bonds formed during the activation process. The integrated intensity of these negative desorption peaks increases slightly at the higher H_2 overpressures, saturating at 30 bar. Comparing the integrated intensity of the negative signal in the range between 2820 and 3150 cm^{-1} to the positive absorbance signal for the activated sample indicates that only ∼3% of the covalent bonds formed by activation are desorbed by subsequently charging the sample at room temperature with 46 bar of H_2. This low percentage of desorption for the 2820−3150 cm^{-1} peaks suggests that a large fraction of covalent bonds (C−H or C−OH) still remain bound to the carbon surface and would be unavailable to accept new H atoms via spillover.

While the major desorption peaks (downward pointing) in Figure 7C correspond directly to the most prominent absorbance peaks observed for the activated sample (3142, 3050, 2820, and 1406 cm^{-1}), we also observe a small desorption peak at 1360 cm^{-1} that appears as a weak shoulder on the low-energy side of the 1406 cm^{-1} desorption peak. This peak is labeled with an asterisk in Figure 7C and is highlighted in the narrower spectral window shown in the Figure 7C inset. Kubota et al. observed a similar peak at 1330 cm^{-1} for H_2-charged ruthenium particles, which they assigned to a species consisting of one H atom bridging two Ru atoms.[40] Thus, we assign the negative peak at 1360 cm^{-1} to the reorganization and/or desorption of "bridging" H atoms initiated by the high molecular H_2 overpressure. This peak is obscured in the absorbance spectrum of the activated sample in Figure 7B because of the very strong 1406 cm^{-1} peak. By Le Chatelier's principle, it is unlikely that the bridging species desorb as H_2 molecules, since the high overpressure of H_2 would favor an equilibrium that is shifted toward the surface-bound species. Instead, we suggest that the gas-phase H_2 molecules dissociate on the activated Ru NP surfaces, further saturating the NP surface with H atoms and causing the bridging H atoms to rearrange to on-top configurations. This observation gives a direct piece of spectroscopic evidence for the room temperature dissociation of H_2 molecules necessary for the spillover process on the Ru-BC_X sample.

We now turn to the *positive absorbance peaks* observed upon H_2 charging of the activated Ru-BC_X sample (Figure 7C). The only positive-going peaks observed in Figure 7C are in the range of ∼3500−6000 cm^{-1} and are indicative of molecular H_2 physisorption, as discussed above. Importantly, we do not observe any peaks in the range of ∼3400 cm^{-1} or below 1300 cm^{-1}, indicating that the activation process has hindered the subsequent formation of both surface hydroxyls (3400 cm^{-1} range) and the proposed spillover C−H species giving rise to the peaks below 1300 cm^{-1}. Since the carbon surface is populated with a large proportion of covalent C−H or C−OH bonds (2820−3150 cm^{-1}/1406 cm^{-1}) after the activation process, these carbon atoms are no longer available to accept H atoms migrating from adjacent Ru NPs, therefore explaining the lack of weakened, spillover-induced C−H bonds below 1300 cm^{-1}. In contrast, the activation process does not hinder the physisorption of molecular H_2, since the physisorption process is not mediated through any specific adsorption sites. Instead, physisorption is nonspecific and only requires appreciable surface area and pore structure, which is not compromised by the activation process. The lack of peaks below 1300 cm^{-1} for the H_2-charged activated Ru-BC_X sample gives further evidence that the mechanism giving rise to these peaks is distinct from the physisorption process and that these peaks arise only when appreciable unbound carbon atoms are available on the carbon surface. This conclusion lends further support to our assignment of the 1070 cm^{-1}/1230 cm^{-1} peaks as bending modes of weakened C−H bonds formed on the carbon acceptor substrate via a spillover process.

In a final attempt to confirm the assignment of the low-energy peaks as arising from vibrational modes of weakened C−H bonds, we performed inelastic neutron scattering (INS) experiments to compare with the DRIFTS spectra. Figure 8 shows the INS spectrum of the Ru-BC_X sample following room temperature H_2 charging at 22 bar. A series of broad peaks are

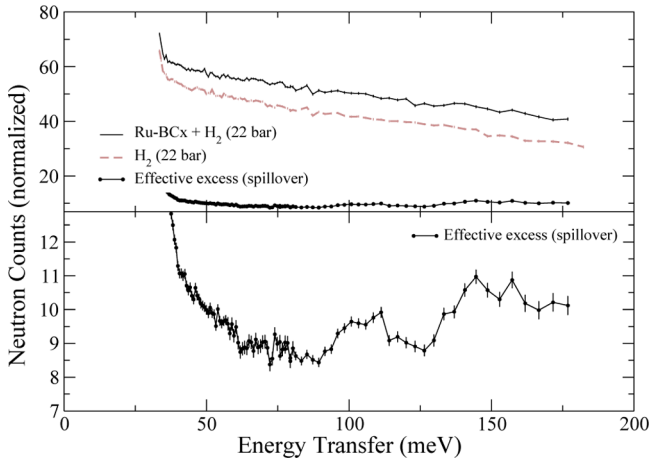

Figure 8. (upper) INS spectra of the Ru-BC_X sample charged with hydrogen at room temperature (solid black line) compared to the scattering from hydrogen gas charged to the same pressure (brown, dashed line). Error bars, representing one standard deviation, are small due to the 2 days counting time and the need to subtract large numbers to obtain the spillover excess scattering after subtracting all other components of the spectrum (black filled circles). The lower panel shows the spillover component in detail.

dx.doi.org/10.1021/jp305235p | J. Phys. Chem. C 2012, 116, 26744−26755

observed between 100 and 200 meV energy transfer, with distinct peaks at 105, 140, and 160 meV (807, 1129, and 1290 cm^{-1}). These peaks arise from inelastic scattering of neutrons, in which energy is lost through the excitation of vibration−rotation transitions, a process similar to Raman spectroscopy. Importantly, the peaks observed at 140 and 160 meV are very close in energy to the peaks observed in the DRIFTS experiment at 1070 and 1230 cm^{-1}, respectively. This encouraging similarity indicates that both measurements are capable of detecting the species that we have assigned to spillover C−H bonds. Figure 9 plots the calculated INS spectrum for the graphene-H fragment shown in Figure 5a. The calculated spectrum shows two distinct peaks at 110 and 150 meV that correspond to the bending motions of basal plane bound C−H bonds. Again, these peak energies are very close to those observed in both the DRIFTS and INS experiments and lend further support to the hypothesis that ruthenium-mediated spillover gives rise to surface-bound C−H bonds on the adjacent carbon substrate and that these bonds can be observed via both optical and neutron vibrational spectroscopies. Finally,

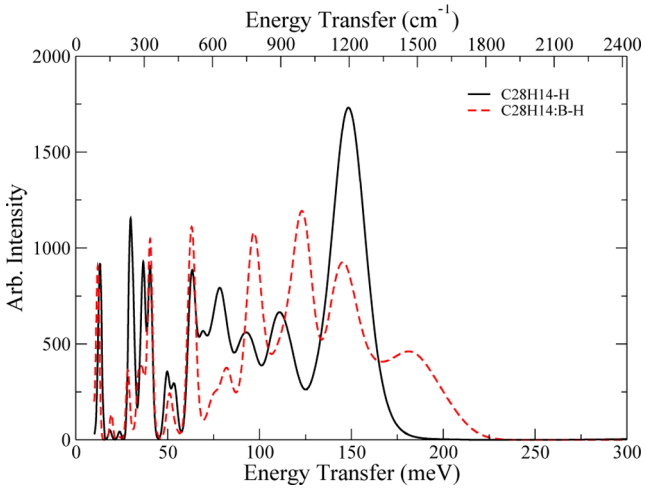

Figure 9. Predicted INS spectra for graphene molecular fragments as in Figure 5 (black line). The neutron scattering spectra have been weighted for the scattering cross section of hydrogen, and the atomic displacement of the vibration of hydrogen only to correspond to the difference spillover curve presented in Figure 8. Exchanging a central carbon atom for boron has a strong influence on the hydrogen modes at higher energies (red dashed line).

we note the striking similarity of the INS spectra shown in Figure 8 to the spectra observed for hydrogen-terminated disordered graphitic carbons in a previous study, which also assigned these peaks to C−H bending vibrations.[39] This agreement lends further support to our assignment of the ∼110 meV and ∼150 meV peaks in both INS and DRIFTS spectra to C−H bonds formed via spillover. This is in contrast to the riding mode enhancements due to atomic hydrogen seen in another study.[40]

CONCLUSION

The rigorous experimental and theoretical analysis described here leads us to interpret that decoration of a boron-doped carbon sample with small (1−3 nm) Ru NPs enables the realization of ruthenium-mediated spillover of H atoms onto the carbon substrate. This interpretation is driven by the observation of a characteristic set of infrared absorbance peaks in the *in situ* DRIFTS experiment, the primary peaks belonging to the stretching mode (2770 cm^{-1} for C−H and 2010 cm^{-1} for C−D) and the bending mode (1230 cm^{-1}/1070 cm^{-1} for C−H and 920 cm^{-1} (broadened) for C−D). Each of these modes is observed at energies close to, but lower in energy than, the energies predicted by first-principles calculations. This reduced energy suggests that the proposed C−H/C−D bonds formed by spillover on the Ru-BC_X sample are weaker than covalent bonds with idealized sp^3 bond angles and likely occupy carbon sites experiencing local strain or deformation.

Our analysis does not allow us to quantify the amount of hydrogen spillover onto the carbon substrate. However, we only observe a relatively small (∼18%) increase of the hydrogen sorption capacity for the Ru-BC_X sample relative to the BC_X sample. This increase is much smaller than that previously observed for spillover samples that fall in the range of 2× to 10× enhancements.[9−11] Our analysis also does not allow us to quantify how far from the Ru NPs the spillover H atoms are able to diffuse at room temperature. However, we do note that we can estimate a bond energy of ∼10−20% lower than a covalent C−H bond with near-ideal sp^3 bond angles, and furthermore, the peaks we attribute to spillover hydrogen are completely reversible. These estimated bond energies are too high to allow for significant diffusion of H atoms at room temperature on carbon surfaces. This realization, in conjunction with the low spillover-related enhancement observed in Figure 2, leads us to conjecture that the H atoms spilled over onto the substrate in the Ru-BC_X sample likely do not diffuse far from the Ru NPs. Thus, in our materials, the data suggest a spillover process where a small "pool" of hydrogen atoms dissociate and are directly adjacent to the Ru NPs, which can subsequently recombine effectively with other adjacent hydrogen atoms to desorb from the Ru NPs in the reverse recombination process. Other recently proposed mechanisms are also plausible, including a mechanism involving the diffusion of physisorbed H[14,19] atoms to form "islands" around localized surface functional groups (e.g., surface oxides),[41] followed by Eley−Rideal recombination in the desorption step.[14] Further clarification of the mechanism(s) involved for spillover in these materials will require additional DRIFTS measurements on samples with varying metal NP dispersion and surface functionality.

ASSOCIATED CONTENT

Supporting Information

Comparison of infrared vibrational energies for H atoms on undoped and doped boron-doped graphene fragments. This material is available free of charge via the Internet at http://pubs.acs.org.

AUTHOR INFORMATION

Corresponding Author

*E-mail: jeffrey.blackburn@nrel.gov.

Notes

The authors declare no competing financial interest.

ACKNOWLEDGMENTS

NREL authors gratefully acknowledge research support from the U.S. Department of Energy, Office of Energy Efficiency and Renewable Energy, Fuel Cell Technologies Program, under Contract No. DE-AC36-08-GO28308 with the National Renewable Energy Laboratory. C.M. Brown and M. Hudson

acknowledge financial support from the U.S. Department of Energy under Grant nos. DE-EE0002978 and DE-AI-01-05EE11104 through the EERE Fuel Cell Technology Program. J-D R. Rocha and J.L. Blackburn also thank the U.S. Department of Defense, HQ Defense Logistics Agency, for funding the initial setup of the DRIFTs instrument, under Agreement no. SP10010800307.

REFERENCES

(1) Satyapal, S.; Petrovic, J.; Read, C.; Thomas, G.; Ordaz, G. *Catal. Today* **2007**, *120*, 246−256.
(2) Also see the Final Reports for the DOE "Metal Hydride", "Chemical Hydrogen Storage", and "Hydrogen Sorption" Centers of Excellence: http://www1.eere.energy.gov/hydrogenandfuelcells/hydrogen_publications.html-h2_storage.
(3) Sakintuna, B.; Lamari-Darkrim, F.; Hirscher, M. *Int. J. Hydrogen Energy* **2007**, *32*, 1121−1140.
(4) Hamilton, C. W.; Baker, R. T.; Staubitz, A.; Manners, I. *Chem. Soc. Rev.* **2009**, *38*, 279−293.
(5) Murray, L. J.; Dinca, M.; Long, J. R. *Chem. Soc. Rev.* **2009**, *38*, 1294−1314.
(6) Fierro, V.; Szczurek, A.; Zlotea, C.; Mareche, J. F.; Izquierdo, M. T.; Albiniak, A.; Latroche, M.; Furdin, G.; Celzard, A. *Carbon* **2010**, *48*, 1902−1911.
(7) Zhao, W.; Fierro, V.; Zlotea, C.; Aylon, E.; Izquierdo, M. T.; Latroche, M.; Celzard, A. *Int. J. Hydrogen Energy* **2011**, *36*, 5431−5434.
(8) Wang, L.; Yang, R. T. *Energy Environ. Sci.* **2008**, *1*, 268−279.
(9) Li, Y.; Yang, R. T. *J. Phys. Chem. C* **2007**, *111*, 11086−11094.
(10) Li, Y.; Yang, R. T. *J. Am. Chem. Soc.* **2006**, *128*, 726−727.
(11) Li, Y.; Yang, R. T. *J. Am. Chem. Soc.* **2006**, *128*, 8136−8137.
(12) Conner, W. C.; Falconer, J. L. *Chem. Rev.* **1995**, *95*, 759−788.
(13) Prins, R. *Chem. Rev.* **2012**, *112*, 2714−2738.
(14) Psofogiannakis, G. M.; Froudakis, G. E. *Chem. Commun.* **2011**, *47*, 7933−7943.
(15) Wang, Z.; Yang, F. H.; Yang, R. T. *J. Phys. Chem. C* **2010**, *114*, 1601−1609.
(16) Singh, A. K.; Ribas, M. A.; Yakobson, B. I. *ACS Nano* **2009**, *3*, 1657−1662.
(17) Stadie, N. P.; Purewal, J. J.; Ahn, C. C.; Fultz, B. *Langmuir* **2010**, *26*, 15481−15485.
(18) Lin, Y.; Ding, F.; Yakobson, B. I. *Phys. Rev. B* **2008**, *78*, 041402.
(19) Chen, L.; Cooper, A. C.; Pez, G. P.; Cheng, H. *J. Phys. Chem. C* **2007**, *111*, 18995−19000.
(20) Spoto, G.; Vitillo, J. G.; Cocina, D.; Damin, A.; Bonino, F.; Zecchina, A. *Phys. Chem. Chem. Phys.* **2007**, *9*, 4992−4999.
(21) FitzGerald, S. A.; Allen, K.; Landerman, P.; Hopkins, J.; Matters, J.; Myers, R.; Rowsell, J. L. C. *Phys. Rev. B* **2008**, *77*, 224301.
(22) FitzGerald, S. A.; Burkholder, B.; Friedman, M.; Hopkins, J. B.; Pierce, C. J.; Schloss, J. M.; Thompson, B.; Rowsell, J. L. C. *J. Am. Chem. Soc.* **2011**, *133*, 20310−20318.
(23) Farha, O. K.; Wilmer, C. E.; Eryazici, I.; Hauser, B. G.; Parilla, P. A.; O'Neill, K.; Sarjeant, A. A.; Nguyen, S. T.; Snurr, R. Q.; Hupp, J. T. *J. Am. Chem. Soc.* **2012**, *134*, 9860−9863.
(24) Udovic, T. J.; Brown, C. M.; Leao, J. B.; Brand, P. C.; Jiggetts, R. D.; Zeitoun, R.; Pierce, T. A.; Peral, I.; Copley, J. R. D.; Huang, Q.; Neumann, D. A.; Fields, R. J. *Nucl. Instrum. Methods Phys. Res., Sect. A* **2008**, *588*, 406−413.
(25) Azuah, R. T. *J. Res. Natl. Inst. Stand. Technol.* **2009**, *114*, 341.
(26) Becke, A. D. *J. Chem. Phys.* **1993**, *98*, 5648−5652.
(27) Binkley, J. S.; Pople, J. A.; Hehre, W. J. *J. Am. Chem. Soc.* **1980**, *102*, 939−947.
(28) Frisch, M. J.; et al. *Gaussian 09, Revision A.1*; Gaussian, Inc.: Wallingford, CT, 2009.
(29) Stuckert, N. R.; Wang, L.; Yang, R. T. *Langmuir* **2010**, *26*, 11963−11971.
(30) Wang, L.; Stuckert, N. R.; Chen, H.; Yang, R. T. *J. Phys. Chem. C* **2011**, *115*, 4793−4799.
(31) Elko-Hansen, T. D. M.; McCrate, J. M.; Ekerdt, J. G. *J. Phys. Chem. C* **2011**, *115*, 9048−9052.
(32) Pylypenko, S.; Queen, A.; Olson, T. S.; Dameron, A.; O'Neill, K.; Neyerlin, K. C.; Pivovar, B.; Dinh, H. N.; Ginley, D. S.; Gennett, T.; O'Hayre, R. *J. Phys. Chem. C* **2011**, *115*, 13676−13684.
(33) Zhou, Y.; Neyerlin, K.; Olson, T. S.; Pylypenko, S.; Bult, J.; Dinh, H. N.; Gennett, T.; Shao, Z.; O'Hayre, R. *Energy Environ. Sci.* **2010**, *3*, 1437−1446.
(34) Acharya, C. K.; Sullivan, D. I.; Turner, C. H. *J. Phys. Chem. C* **2008**, *112*, 13607−13622.
(35) Zhao, Y.; Kim, Y.-H.; Dillon, A. C.; Heben, M. J.; Zhang, S. B. *Phys. Rev. Lett.* **2005**, *94*, 155504.
(36) Stoicheff, B. P. *Can. J. Phys.* **1957**, *35*, 730.
(37) Zhao, W.; Fierro, V.; Zlotea, C.; Izquierdo, M. T.; Chevalier-Cesar, C.; Latroche, M.; Celzard, A. *Int. J. Hydrogen Energy* **2012**, *37*, 5072−5080.
(38) Papanek, P.; Kamitakahara, W. A.; Zhou, P.; Fischer, J. E. *J. Phys.: Condens. Matter* **2001**, *13*, 8287−8301.
(39) Mitchell, P. C. H.; Ramirez-Cuesta, A. J.; Parker, S. F.; Tomkinson, J.; Thompsett, D. *J. Phys. Chem. B* **2003**, *107*, 6838.
(40) Kubota, J.; Aika, K.-i. *J. Chem. Soc., Chem. Commun.* **1992**, 661.
(41) Psofogiannakis, G. M.; Froudakis, G. E. *J. Am. Chem. Soc.* **2009**, *131*, 15133−15135.